Ceramics International 49 (2023) 12415–12422

Contents lists available at ScienceDirect

Ceramics International

journal homepage: www.elsevier.com/locate/ceramint

Phosphate and buffer capacity effects on biomimetic carbonate apatite

Stephanie L. Wong, Alix C. Deymier *

Department of Biomedical Engineering, University of Connecticut Health Center, 263 Farmington Ave, Farmington, CT, 06030, USA

ARTICLE INFO

Keywords:
B) spectroscopy
(D) apatite
(E) biomedical applications
(B) maturation

ABSTRACT

With the increasing use of carbonated apatite (CAp) in biomedical devices, it has become necessary to understand how this thermodynamically unstable mineral interacts with varying surrounding body fluids. Despite existing knowledge about the evolution of other calcium phosphates in bio-like fluids, it is unknown how CAp reacts in these solutions. Therefore, our goal was to determine how solution phosphate concentration and the buffer capacity (BC) affects CAp dissolution/recrystallization. To do so, CAp powder was first synthesized through an aqueous precipitation reaction and then exposed to one of the following solutions for 3 days: (1) 0 mM PO4, (2) 8 mM PO4, (3) 16 mM PO4, (4) low BC, or (5) high BC. Afterwards, the powders were analyzed for mass loss, composition via Raman, crystal structure via XRD, and size via TEM. The solutions were evaluated for Ca, P, Na, and K through ICPOES. Our results suggest that increased phosphate in the solution, regardless of BC, created larger, more crystalline CAp crystals, indicating crystal maturation. In addition, the crystals had fewer carbonate substitutions and more phosphate ion uptake from the solution after pH equilibrium. This data offers insight on how CAp in biomaterials may mature and change composition and material properties in the body after implantation.

1. Introduction

The ability of apatites to mimic biological mineral, in addition to their tunability via ionic substitution, makes them ideal as restorative biomaterials for bone and teeth [1–4]. Carbonate-substituted apatites are of particular interest as carbonate makes up ~2–8 wt% of biomineral in those tissues [5,6]. Substitution of carbonate for either phosphate (PO_4^{3-}) or hydroxyl (OH^-) groups in the apatite structure, known as B- and A-type respectively [7,8], introduces disorder in the crystal lattice. This makes carbonated apatite (CAp) formation unfavorable compared to stoichiometric hydroxyapatite (HA) according to classical thermodynamics. As a result, the crystals exhibit reduced growth and maturation, increased lattice strain, decreased crystal size, crystallinity, and elastic modulus as well as increased solubility [9–14]. The thermodynamic instability, or relative immaturity, of CAp is also expected to increase the reactivity of CAp to surrounding solutions, suggesting a possible evolution of CAp towards hydroxyapatite-like compositions and structures during solution exposure [11].

Previous studies investigating the effects of phosphate saturated solutions on non-apatitic calcium phosphates have shown that factors such as solution pH, ionic concentration, and solution composition affect the mineral's propensity for phase transformation and maturation into hydroxyapatite [15–19]. However, despite its current use as a biological agent, it remains unknown how CAp-based biomaterials change when exposed to phosphate-rich solutions, such as phosphate buffered saline (PBS), during storage or implantation [20–24]. The two main factors of concern are (1) the role of phosphate concentration on substitutional ion exchange in apatites, especially with regards to carbonate, and (2) the effect of varied buffering capacity on the apatite composition and structure. Therefore, this study evaluated the dissolution/recrystallization of biomimetic CAp after exposure to varying phosphate concentrations and BC. Shedding light on the mechanism will provide insight on how the material properties of CAp may change when used in biomedical scaffolds.

2. Methods

2.1. Apatite synthesis

To recreate the carbonate levels seen in bone and dentin, carbonated

Abbreviations: BC, Buffer Capacity; PBS, Phosphate Buffered Saline.

* Corresponding author. UCH-Dept. of Biomedical Engineering, University of Connecticut School of Dental Medicine, 263 Farmington Avenue (Mail Code: 1721), Farmington, CT, 06030, USA.
E-mail address: deymier@uchc.edu (A.C. Deymier).

https://doi.org/10.1016/j.ceramint.2022.12.101
Received 7 July 2022; Received in revised form 1 December 2022; Accepted 12 December 2022
Available online 14 December 2022

Table 1
Solution composition for the effect of PO_4^{3-} and BC.

	Effect of PO_4^{3-}			Effect of BC	
Solution Used	0.1 M KCl	0.7x PBS	0.017 M KH_2PO_4 + 0.083 M KCl	1x PBS	0.012 M KH_2PO_4 + 0.16 M KCl
Ionic Strength	0.1 M	0.1 M	0.1 M	0.017 M	0.017 M
pH	3.0	3.0	3.0	6.6	6.6
Buffering Capacity	n/a	n/a	n/a	**5.2×10^{-3} (Low)**	**7.4×10^{-3} (High)**
PO_4^{3-} Content	**0 mM**	**8 mM**	**16 mM**	12 mM	12 mM

apatite with 6 wt% carbonate content was synthesized via aqueous precipitation as previously described [21]. The mineral phase was confirmed to be carbonated apatite via Raman spectroscopy, Fourier Transform Spectroscopy, and X-ray Diffraction (Figs. S1a–c). Carbonate content was analyzed through Raman spectroscopy and compared against our CAp standards.

2.2. Solutions

Solutions were prepared to allow us to independently measure the effect of phosphate content and BC while keeping all other factors constant (Table 1). To determine the effect of phosphate content independent of buffering capacity, we compared: (1) 0 mM PO_4^{3-} (0.1 M KCl, Sigma-Aldrich), (2) 8 mM PO_4^{3-} (0.7x PBS, Fisher), and (3) 16 mM PO_4^{3-} (0.017 M KH_2PO_4 with 0.083 M KCl, Sigma-Aldrich). These solutions all exhibited an ionic strength of 0.1 M and were titrated to pH 3 with 0.1 M HCl to negate buffer capacity effects.

To isolate the effect of BC, we compared solutions with variable buffering capacities (BC) of: (1) BC = 5.2×10^{-3} (1X PBS) and (2) BC = 7.4×10^{-3} (0.012 M KH_2PO_4 with 0.16 M KCl). Solutions (1) and (2) both have a phosphate concentration of 0.12 M PO_4^{3-}, 0.17 M ionic strength, and a pH of 6.6.

2.3. Powder exposure to solutions

For all conditions, 50 mg of CAp powder was placed in a conical tube containing 10 mL of the solution of interest (Fig. S2). The tube was agitated for 72 h during which the pH was taken throughout. Afterwards, the powders were filtered, thoroughly rinsed, and dried in a 60 °C oven overnight. Once cooled, each powder sample was massed to determine the change in mass (Δmass). Each condition was performed in triplicate.

2.4. Raman spectroscopy

Powder composition was determined via Raman spectroscopy. Using a WiTec Raman microscope with a 785 nm laser, 10 spectra were collected per sample using a 50x objective and an integration time of 30× 1-s per spectra. The WiTec Project 5 software was used to deconvolute the v_1 PO_4^{3-} (950 cm^{-1}), v_1 PO_4^{3-} (960 cm^{-1}), and v_1 CO_3^{2-} (1070 cm^{-1}) peaks using a Gaussian fit function. To determine the carbonate to phosphate ratio (CO3/PO4), the 1070 peak area was divided by the sum of the 950 and 960 peak areas (1070/950 + 960). Values were averaged over all 10 spectra for each sample including exposed and non-exposed powder samples. The difference in CO3/PO4 ratio between unexposed and exposed powders was calculated for each condition and will be reported as the percent change in CO3/PO4 (ΔCO3/PO4).

2.5. X-ray diffraction

X-ray diffraction (XRD) was used to determine the phase and structural lattice changes of the powders after exposure. A Bruker D2 Phaser X-Ray Diffractometer (Bruker AXS, Germany) operating at 30 kV and 10 mA with an acquisition time of 1.0 s/increment and an increment of 0.02° ranging from 20 to 60° (2θ) was employed to obtain the peaks of interest. PseudoVoigt peak fitting functions were used to identify peak centers and integral breadth with the Diffrac.eva analysis software. The powders were compared with the Powder Diffraction File (PDF) open database from the International Center for Diffraction Data (ICDD) to identify and confirm the apatite mineral phase and possible secondary phases, such as brushite. The changes in d-spacing of the 002 (Δ002), 310 (Δ310), and 004 (Δ004) peaks were calculated and averaged between the pre- and post-exposure samples to determine changes in crystal lattice parameters (n = 3). The coherent domain size (CDS) and microstrain (με) were calculated via the Halder-Wagner method using the integral breadth of the peaks to determine the average changes in crystal size and lattice structure.

2.6. ICP-OES

One sample from each condition (n = 1) was analyzed for changes in calcium (Ca), phosphorus (P), sodium (Na), and potassium (K) before and after solution exposure via a PerkinElmer 7300DV Dual View Inductively Coupled Plasma–Optical Emission Spectrometer (ICP-OES). All samples were directly analyzed at 20x dilution due to the very high levels of phosphate in the samples. Standard quality assurance procedures were employed, including analysis of initial and continuing calibration checks and blanks, duplicate samples, preparation blanks (Blank), post digestion spiked samples, and laboratory control samples (LCS).

2.7. Transmission Electron Microscopy

Transmission electron microscopy (TEM) was used to determine the size and morphology of the crystals. For each condition, 2 mg of powder was added to 1 mL of 100% ethanol, sonicated for 90 min, and dropped onto lacey carbon TEM grids. The crystals were imaged under Bright Field TEM on a Tecnai T-12 instrument operating at 120 kV and 310 kX magnification with 1.28 s acquisition time. The average crystal size and the size distribution were obtained from 7 representative images, a total of 225 crystals, for each condition. The change in crystal size was calculated by comparing the average sizes of the exposed versus non-exposed crystals.

2.8. Statistical and correlation analysis

One-way Analysis of Variance (ANOVA) with a Tukey pairwise comparison was used in Minitab (Minitab, LLC, State College, Pennsylvania, USA) to determine the statistical significance between each condition. Significance is defined as $p < 0.05$.

Pearson correlation coefficients were used to determine the association between the independent variables and the outcomes from Raman, XRD, mass, and pH of all samples (n = 3). Significance is defined as $p < 0.05$ and correlations are denoted as c.

3. Results

3.1. Carbonate apatite pre-exposure

The synthesized mineral is clearly a B-type carbonate substituted apatite as indicated by the characteristic PO_4^{3-} and CO_3^{2-} peaks in the Raman and FTIR spectra (Figs. S1a–b) [5,10,25,26]. The average carbonate content as determined from Raman was 6.4%. The XRD patterns confirmed the apatitic structure with no additional crystalline phases within the powder (Fig. S1c). The average coherent domain size of the powders was 2.70 nm as determined by the Halder-Wagner equation and the average crystal size was 21.17 ± 7.79 nm through TEM. The

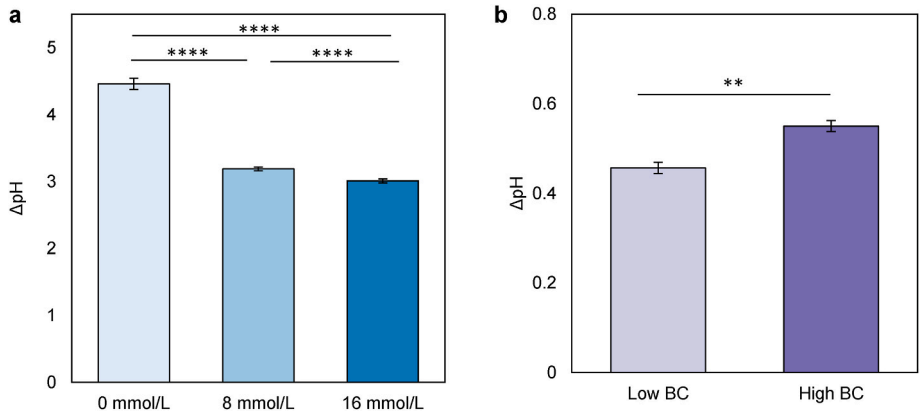

Fig. 1. (a) ΔpH decreased after exposure to varying phosphate concentrations while **(b)** ΔpH increased as buffer capacity increased after exposure. $p < 0.05$.

Table 2
Correlations for the phosphate conditions.

	%Δ Mass	% Δ CO3/PO4	Δ pH	002	310	004	Δ002	Δ310	Δ004	ΔCDS	Δμε
mM PO_4^{3-}	−0.66	−0.91	−0.91	−0.30	0.16	−0.71	−0.21	0.53	0.87	0.87	−0.84
%Δ Mass		0.86	0.90	−0.26	−0.64	0.11	−0.30	−0.72	−0.21	−0.34	0.36
% Δ CO3/PO4			0.98	−0.01	−0.48	0.45	−0.09	−0.75	−0.64	−0.64	0.62
ΔCDS			−0.66	−0.50	−0.15	−0.76	−0.42	0.22	0.87		−0.99
Δμε			0.65	0.49	0.16	0.74	0.42	−0.19	−0.81	−0.99	

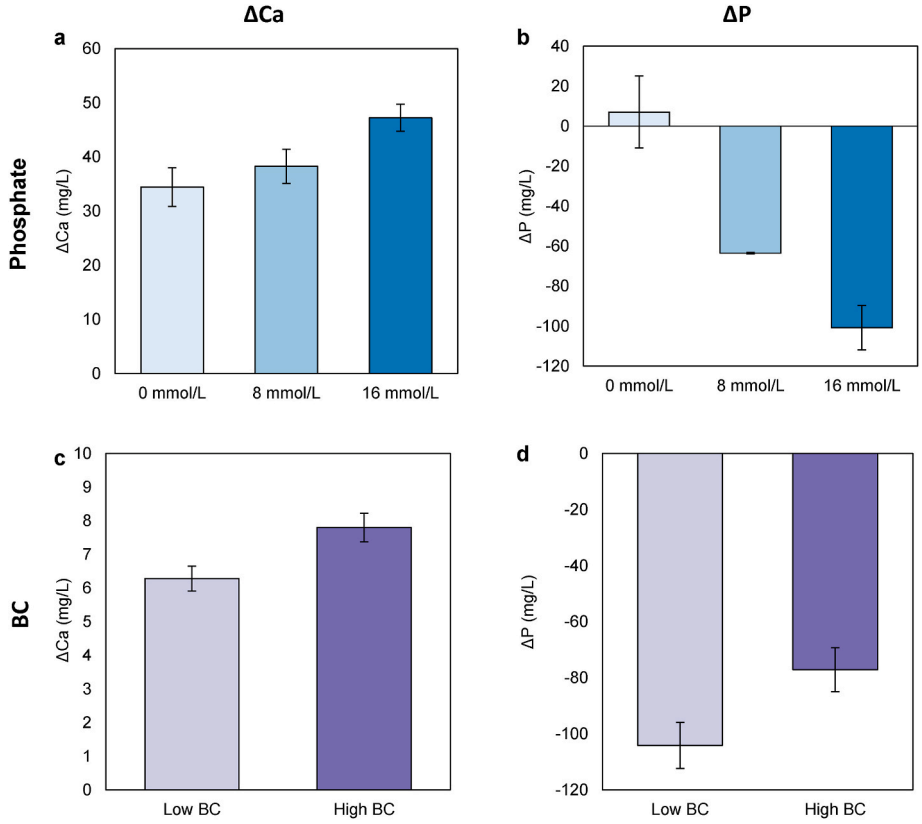

Fig. 2. (a–b) ICP-OES data of ΔCa and ΔP solutes after powder exposure for the phosphate solutions and **(c–d)** buffer capacity conditions. (n = 1) Note: **(b)** has small instrumental error bars.

differences between the coherent domain size and the average crystal size indicate the synthesized powders are polycrystalline. An estimated specific surface area (SSA) of 72.19 m^2/g was calculated from the TEM measurements assuming that the platelets are ellipsoidal and have a density of 3.03 g/cm^3 [27]. This average SSA was consistent for all powders used in this study thus eliminating surface area as a variable.

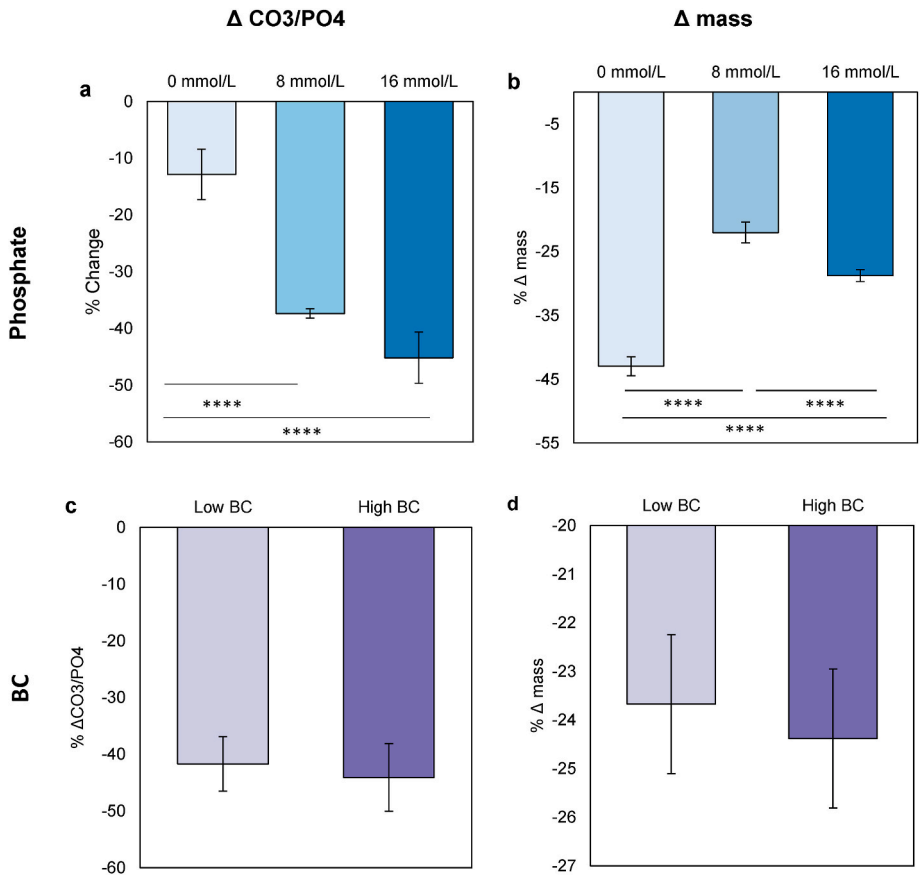

Fig. 3. (a–b) The ΔCO3/PO4 and Δmass of the powders decreased in the phosphate solutions and **(c–d)** buffer capacity solutions. Significance is $p < 0.05$.

3.2. The effect of phosphate

3.2.1. Composition

All solutions exhibited an increase in pH and achieved a steady state pH during the first hour of exposure to the CAp powders (Fig. 1a, Fig. S3a). The 0 mM PO_4^{3-} solution had the highest ΔpH of 4.46, while 8 and 16 mM PO_4^{3-} had ΔpH's of 3.19 and 3.01, respectively. Overall, ΔpH significantly decreased as solution PO_4^{3-} concentration increased ($c = -0.91$; Table 2).

Solution Ca levels generally increased with increasing solution PO_4^{3-} levels (Fig. 2a). The opposite trend occurred for ΔP, where ΔP decreased in the solution as initial PO_4^{3-} content increased (Fig. 2b). Solution ΔNa did not change significantly with solution PO_4^{3-} (Fig. S4a). ΔK generally increased in 0 mM and 8 mM PO_4^{3-} solution and decreased in the 16 mM PO_4^{3-} solution after powder exposure (Fig. S4b).

The CO3/PO4 ratio significantly decreased in all CAp powders after solution exposure as phosphate concentration increased (Fig. 3a). The ΔCO3/PO4 exhibited a strong negative correlation with solution PO_4^{3-} concentration ($c = -0.91$; Table 2). 16 mM PO_4^{3-} had the greatest ΔCO3/PO4 with 45% decrease while the 0 mM PO_4^{3-} condition had a 12% decrease.

3.2.2. Structure

All CAp powders exhibited mass loss after solution exposure (Fig. 3b). The greatest mass loss (−42.9%) occurred in the solution with 0 mM PO_4^{3-}, with the smallest loss occurring in the 8 mM PO_4^{3-} solution (−22%). The change in mass (Δmass) generally had a negative correlation with PO_4^{3-} ($c = -0.66$, Table 2).

There were no apparent mineral phases other than hydroxyapatite in all conditions. The change in the c-axis d-spacing, Δ002, did not change in the 0 mM PO_4^{3-} condition and showed no clear trend in the PO_4^{3-} solutions, with the highest average change being 0.005 nm out of all conditions (Fig. 4a). Similarly, Δ310 did not change significantly in the 0 mM PO_4^{3-} condition, whereas it increased for the other PO_4^{3-} solutions to about 0.006 Å (Fig. 4b). Δ002 or Δ310 was only weakly correlated to PO_4^{3-} content ($c = -0.21$ and $c = 0.53$, respectively; Table 2). The CDS increased for all solutions (Fig. 5a). CAp in 16 mM PO_4^{3-} had the highest ΔCDS with 1.44 nm increase compared to the other conditions where 0 mM and 8 mM PO_4^{3-} increased by 0.67 and 0.87, respectively. ΔCDS was strongly correlated to the amount of PO_4^{3-} ($c = 0.87$; Table 2). Conversely, the Δμε was negative for all solutions, with a significant decrease in Δμε 16 mM PO_4^{3-} compared to the 0 mM PO_4^{3-} ($c = -0.84$; Table 2; Fig. 5b).

The average crystal size as measured by TEM also increased for all conditions, ranging from 0.57 to 1.81 nm in growth. The change in crystal size for 0 mM, 8 mM, and 16 mM PO_4^{3-} were 1.78, 0.57, and 1.81 nm, respectively. There is no clear trend in size with the amount of PO_4^{3-} in the solution.

3.3. The effect of buffer capacity

3.3.1. Composition

The pH increased by 0.46 and 0.55 for low and high BC, respectively (Fig. 1b). The ΔpH of the high BC solution was significantly higher than low BC. The BC was positively correlated to ΔpH ($c = 0.96$; Table 3).

Solution Ca increased by 6.28 mg/L and 7.80 mg/L for low and high BC, respectively, while solution P decreased by −104.10 mg/L and −77.10 mg/L for low and high BC, respectively (Fig. 2c–d) but the change was not significant. ΔNa decreased in the solution to around −44 mg/L for low BC while there was no change in ΔNa for high BC due to negligible amounts in the initial solution (Fig. S4c). Conversely, ΔK increased in the solution to about 18.90 mg/L for low BC while ΔK

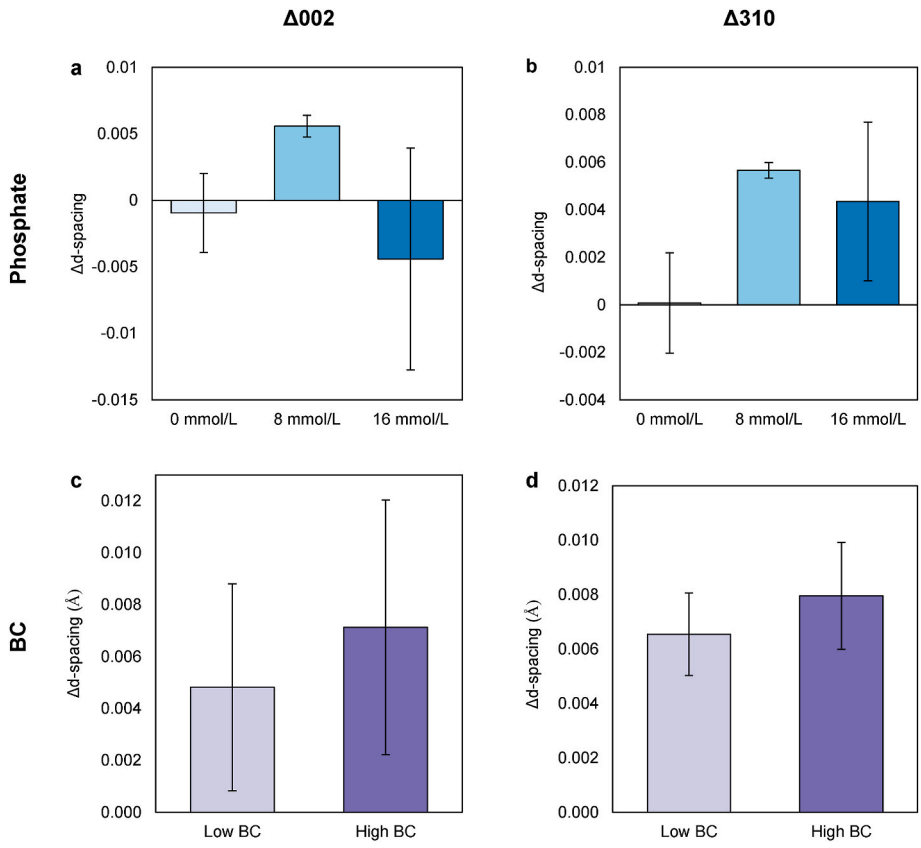

Fig. 4. (a–b) The changes in apatite d-spacing of the 002 and 310 in different phosphate concentrations and **(c–d)** buffer capacities.

generally decreased to −36.00 mg/L in the solution for high BC (Fig. S4d).

The CO3/PO4 decreased by −41% and −44% for low and high BC, respectively, with no statistical significance between BCs (Fig. 3c).

3.3.2. Structure

The powder mass decreased by about −24% of the initial mass for both BCs with no significance between low and high BC (Fig. 3d).

There were no other phases besides hydroxyapatite seen in the XRD patterns. The Δ002 and Δ310 slightly increased with exposure but there was no significant difference in BC (Fig. 4c–d). The average CDS increased by about 2.2 nm while the με decreased by −0.02 for both low and high BC with no statistical significance between them (Fig. 5c–d). In addition, ΔCDS had no correlation with BC (c = 0.13; Table 3).

The average crystal size for the control (unexposed crystals), low BC, and high BC were 21.38, 25.79, and 23.12 nm, respectively (Figs. S6a–b). This resulted in an increase of 4.41 nm for low BC and 1.74 nm for high BC.

4. Discussion

To date, phosphate buffered solutions remain the gold standard for storage and testing of mineralized tissue scaffolds. However, the phosphate concentration and buffering capacity of these solutions varies greatly from those found in body fluids to which the scaffolds will eventually be exposed to. Previous examinations showed that simulated body fluids can cause phase changes from tricalcium phosphate and octacalcium phosphate towards hydroxyapatite stoichiometry [16–18]. However, these studies never investigated the effects of phosphate and BC independently nor their effects on carbonated apatites, making it difficult to identify the role that these different components might play. Thus, in this study, we optimized solutions for exposure experiments to independently measure these two variables.

4.1. Phosphate effect

Phosphate buffered solutions are often used to inhibit phosphate diffusion and demineralization [28,29]. However, it is unclear how PO_4^{3-} concentration in solution affects bone-like mineral dissolution/recrystallization. The dissolution mechanisms of apatite are complex and exhibits numerous mechanisms depending on the mineral structure and solution properties [30]. This study does not seek to identify those mechanisms but does show that exposure of bone-like CAp to solutions containing varying levels of PO_4^{3-} led to mineral dissolution in all cases as determined by a decrease in powder mass post-exposure. As hypothesized, the mineral dissolution resulted in an increase in solution pH likely due to the release of buffering ions. The decrease in powder CO3/PO4 ratios and solution P concentration as well as the positive correlation between ΔCO3/PO4 and ΔpH suggests that CO_3^{2-} may be acting as the dominant buffering moiety [31]. However, if we use the expected powder stoichiometry [12] and the mass loss to predict the ΔpH using the Henderson-Hasselbalch equation, the calculated values for 0, 8, and 16 mM PO4 (3.79, 0.60, and 0.64, respectively) were substantially smaller than the experimental values (4.46, 3.19, and 3.05, respectively). This suggests that carbonate release is not the sole regulator of solution buffering and that contributions from PO_4^{3-} and surface proton sequestration must be considered. We proposed that there may be a 2-step process by which Ca^{2+}, PO_4^{3-}, and CO_3^{2-} moieties are initially released via dissolution, buffering the pH, and establishing an equilibrium between mineral and solution [30]. Then, once ionic equilibrium is established, recrystallization occurs preferentially sequestering available PO_4^{3-} and H^+ while excluding the CO_3^{2-} that continues to buffer [31,32]. We suggest that further studies should examine the ionic concentrations in the solution as a function of time to confirm this possible process.

Further evidence for the dissolution and recrystallization process and its dependence on PO_4^{3-} content comes from the decreased με and

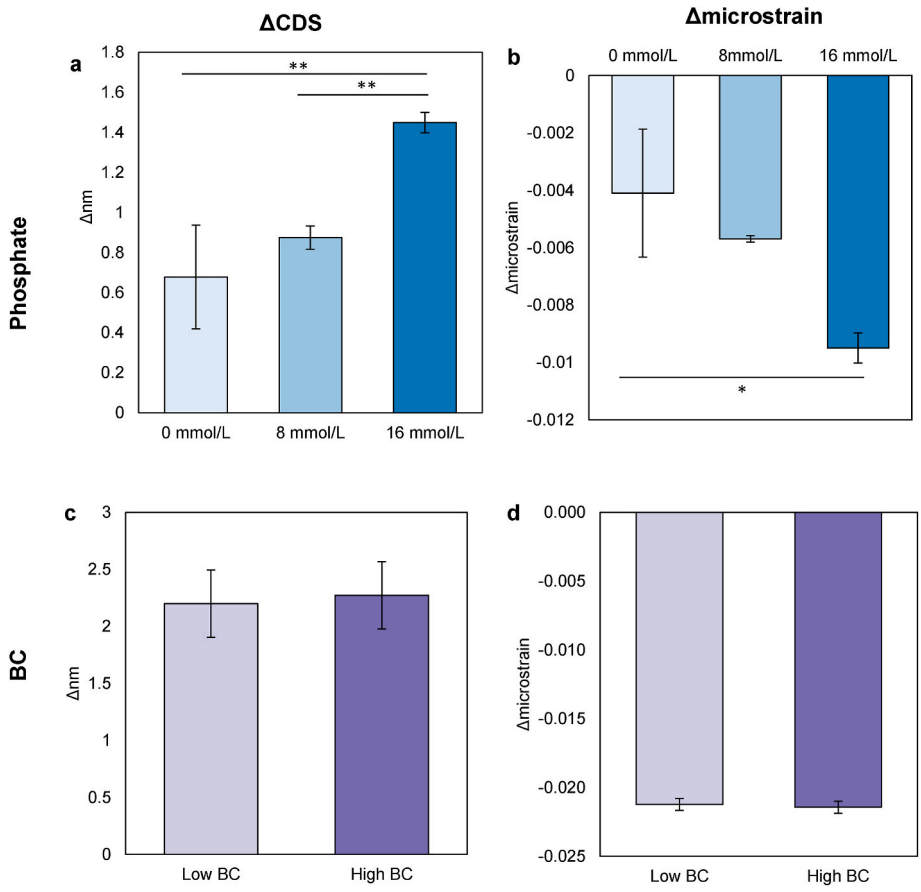

Fig. 5. (a–b) The Δcoherent domain size and Δmicrostrain of CAP in increasing phosphate concentrations and **(c–d)** buffer capacities as determined by the Halder-Wagner method. $p < 0.05$.

Table 3
Correlation for the buffer capacity conditions.

	% Δ Mass	% Δ CO3/PO4	Δ pH	002	310	004	Δ002	Δ310	Δ004	ΔCDS	Δμε
BC	0.18	−0.26	0.96	0.25	0.37	0.09	0.25	0.37	0.09	0.13	−0.19
%Δ Mass		0.38	0.12	0.02	0.06	0.04	0.02	0.06	0.04	−0.25	0.27
% Δ CO3/PO4			−0.33	0.63	0.62	0.73	0.63	0.62	0.73	0.11	0.13
ΔCDS			0.29	0.21	0.20	0.34	0.21	0.20	0.34		−0.97
Δμε			−0.36	−0.05	−0.04	−0.16	−0.05	−0.04	−0.16	−0.97	

increased CDS and crystal size seen with increased PO_4^{3-} after exposure. This suggests that PO_4^{3-} availability promotes the formation of larger, more ordered crystals, with less CO_3^{2-} substitutional defects - in other words, more mature crystals [21,33,34]. This increase in crystal maturity is expected to induce expansion of the c-axis and contraction of the a-axis due to increased level of OH^- into the lattice structure [33,35]. However, this is accompanied by a decrease in CO_3^{2-} substitution, which is expected to decrease c-axis and increase a-axis lattice spacing [7,12,14,21]. Using literature values from studies examining the effects of both CO_3^{2-} and maturation on apatite lattice spacing [12,36], we find that 3 days of maturation as used here is expected to induce a 0.19% increase in the c-axis d-spacing while the measured loss of carbonate should cause a 0.19% decrease in d-spacing. Together these opposite effects likely explain the lack of significant change in (002) d-spacing with exposure and PO_4^{3-} content. Using similar data for the a-axis [12,36], we find that 3 days of maturation should cause a 0.45% decrease in d-spacing while the carbonate loss causes a 0.48% increase. This small difference may explain the greater tendency for an increased (310) d-spacing in the phosphate solutions where there was a greater loss of CO_3^{2-}. Taken together, mineral exposure to solutions with increasing PO_4^{3-} content create more mature crystals with increased grain size and crystallinity as well as decreased CO_3^{2-} content, even at low initial pH's. The formation of these larger more mature crystals will provide significant surfaces for the sequestration of labile phosphates and protons, thus acting as an additional regulator of pH [37].

4.2. BC effect

BC is defined as a solution's ability to resist changes in pH; therefore, we had hypothesized that the solution ΔpH should be reduced with increasing BC. However, the opposite was observed (Fig. 1b). During exposure, powder dissolution was indicated at both high and low BC by mass loss, increased solution Ca, and CO_3^{2-} loss as shown by the decreased ΔCO3/PO4. Release of buffering ions during dissolution is expected to raise the solution pH; however, this ΔpH was higher in the high BC solution than its low BC counterpart. This unexpected result may be explained from the BC vs pH plots of the low and high BC solutions (Fig. S7). In the pH range from 6.6 (initial pH) to 7.15 (final pH for high BC) the BC slope is much shallower for the low BC solution than the high BC solution. Therefore, as the pH rose during dissolution by

0.45 and 0.55 for the low and high BC solutions respectively, the BC underwent a much more significant drop (~2.5X) in the high initial BC solution than the low BC solution suggesting that the initially high BC solution is relatively less able to regulate pH at the final solution pH. As a result, the high buffering solution underwent a great change in ΔpH than the low BC solution.

The rising pH caused by mineral dissolution induced a decrease in the relative difference in BC between solutions. An initial pH 6.6 was selected because it maximized the difference between the high and low conditions (2.2×10^{-3}). However, as the pH increased to ~7.1, the difference in BC between solutions decreased to 8.6×10^{-4} (2.6-fold) in this closed system. As a result, final BCs were more similar to each other than the initial BCs, providing similar environments for the minerals to recrystallize. This may explain the insignificant difference measured between high and low initial BC for mass loss, CO_3^{2-} loss, lattice spacing, Ca^{2+}, and P levels.

As seen in the effect of PO_4^{3-} above, the lattice parameters did not change despite a decrease in CO_3^{2-} after exposure. This suggests that increased maturation with decreased CO_3^{2-} substitution may counteract any changes in lattice spacing. Combining this with the significant increase in CDS, crystal size, and decreased με in both BC conditions, CAp may be undergoing crystal maturation while removing CO_3^{2-} from the lattice regardless of BC.

Together, this data indicates that the initial BC of phosphate solutions does not have a substantial effect on apatite dissolution/recrystallization mechanisms compared to the effect of phosphate. This is contrary to the BC of other solutions, such as soft drinks and acidic organic solutions [38–40]. This is likely due to the closed nature of the experiment and the initial increase of pH upon powder exposure. This data shows that phosphate has a bigger effect on apatite maturation mechanisms than initial BC.

4.3. Limitations

Although the solutions used here were identical in ionic strength and pH, the ionic compositions were variable. The PBS solutions contained Na^+ while the KH_2PO_4 solutions contained significant K^+. These variations are important to consider since apatite and biological mineral can have many ionic substitutions, especially Na^+ and K^+ [41–45]. These cations substitute for Ca^{2+} when CO_3^{2-} is incorporated into the apatite structure to balance the overall charge of the crystal, with Na^+ substitutions being more favorable due to ionic size similarities [43,46–48]. The larger ionic radius of K^+ results in a bigger lattice strain when substituting for Ca^{2+}, which significantly changes the effect on crystallite size, lattice spacing, apatite thermodynamic stability, and growth kinetics of apatite compared to Na^+ substitutions [48–50]. Although this can introduce measurement bias, we believe that the little to no Na^+ and K^+ in the recrystallized apatites are not substantial enough to cause major effects in maturation.

To mimic biological mineral that mainly contains B-type carbonate substitution, the powders used here were predominantly B-type CAp. While A-type CAp is present in lower quantities in bone and dental mineral, examining the role of A-type carbonate in these apatites could be of interest for future studies.

5. Conclusions

CAp is used in many biomedical applications, such as dental and orthopedic implants. Given that CAp is thermodynamically unstable, it is unknown how CAp evolves in solutions saturated with phosphate despite the knowledge of transformation of other calcium phosphates in similar conditions. This study suggests that phosphate ions in the solution, regardless of buffering capacity, is an important component for CAp to mature into larger crystals with less carbonate substitutions and more phosphate once pH equilibrium is achieved. The work presented here provides insight into controlling the extent of crystal maturation of CAp in biomedical scaffolds with specific phosphate concentrations in solution. The mineral-fluid dynamics of this work will help with fine-tuning scaffolds with a desired amount of carbonate, crystallinity, and crystal size during exposure to phosphate fluids, which may ultimately alter the composition and mechanics of the scaffold. These findings will also aid in the understanding the dissolution/recrystallization mechanisms of CAp in both bone and synthetic analogs after exposure to healthy and pathological fluids where phosphate concentrations are modified.

Declaration of competing interest

The authors declare that they have no known competing financial interests or personal relationships that could have appeared to influence the work reported in this paper.

Acknowledgments

We appreciate the Center for Environmental Sciences and Engineering at the University of Connecticut for their Inductively Coupled Plasma - Optical Emission Spectroscopy work. We also acknowledge the Institute of Materials Science and the UConn/Thermo Fisher Scientific Center for Advanced Microscopy and Materials Analysis at the University of Connecticut for their X-ray Diffraction and Transmission Electron Microscopy facilities. SLW was funded in part by the UConn Graduate School. Additional funding came from ACD's startup funds and NSF CAREER grant 2044870. All authors have no other financial or non-financial interests to disclose.

Appendix A. Supplementary data

Supplementary data to this article can be found online at https://doi.org/10.1016/j.ceramint.2022.12.101.

References

[1] S. Von Euw, Y. Wang, G. Laurent, C. Drouet, F. Babonneau, N. Nassif, T. Azaïs, Bone mineral: new insights into its chemical composition, Sci. Rep. 9 (2019) 1–11, https://doi.org/10.1038/s41598-019-44620-6.
[2] A.F. Khan, M. Awais, A.S. Khan, S. Tabassum, A.A. Chaudhry, I.U. Rehman, Raman spectroscopy of natural bone and synthetic apatites, Appl. Spectrosc. Rev. 48 (2013) 329–355, https://doi.org/10.1080/05704928.2012.721107.
[3] G. Penel, C. Delfosse, M. Descamps, G. Leroy, Composition of bone and apatitic biomaterials as revealed by intravital Raman microspectroscopy, Bone 36 (2005) 893–901, https://doi.org/10.1016/j.bone.2005.02.012.
[4] M.J. Rigali, P. V Brady, R.C. Moore, Radionuclide removal by apatite, Am. Mineral. 101 (2016) 2611–2619, https://doi.org/10.2138/am-2016-5769.
[5] Z. Li, J.D. Pasteris, Tracing the pathway of compositional changes in bone mineral with age: preliminary study of bioapatite aging in hypermineralized dolphin's bulla, Biochim. Biophys. Acta Gen. Subj. 1840 (2014) 2331–2339, https://doi.org/10.1016/j.bbagen.2014.03.012.
[6] A.L. Boskey, R. Coleman, Critical reviews in oral biology & medicine: aging and bone, J. Dent. Res. 89 (2010) 1333–1348, https://doi.org/10.1177/0022034510377791.
[7] H. Madupalli, B. Pavan, M.M.J. Tecklenburg, Carbonate substitution in the mineral component of bone: discriminating the structural changes, simultaneously imposed by carbonate in A and B sites of apatite, J. Solid State Chem. 255 (2017) 27–35, https://doi.org/10.1016/j.jssc.2017.07.025.
[8] A.J. Ortiz-Ruiz, J. de D. Teruel-Fernández, L.A. Alcolea-Rubio, A. Hernández-Fernández, Y. Martínez-Beneyto, F. Gispert-Guirado, Structural differences in enamel and dentin in human, bovine, porcine, and ovine teeth, Ann. Anat. 218 (2018) 7–17, https://doi.org/10.1016/j.aanat.2017.12.012.
[9] S. Cazalbou, D. Eichert, X. Ranz, C. Drouet, C. Combes, M.F. Harmand, C. Rey, Ion exchanges in apatites for biomedical application, in: J. Mater. Sci. Mater. Med., Springer, 2005, pp. 405–409, https://doi.org/10.1007/s10856-005-6979-2.
[10] A. Grunenwald, C. Keyser, A.M. Sautereau, E. Crubézy, B. Ludes, C. Drouet, E. Crub Ezy C, B. Ludes, C. Drouet, Revisiting carbonate quantification in apatite (bio) minerals: a validated FTIR methodology, J. Archaeol. Sci. 49 (2014) 134–141, https://doi.org/10.1016/j.jas.2014.05.004.
[11] C. Drouet, M. Aufray, S. Rollin-Martinet, N. Vandecandelaère, D. Grossin, F. Rossignol, E. Champion, A. Navrotsky, C. Rey, Nanocrystalline apatites: the fundamental role of water, Am. Mineral. 103 (2018) 550–564, https://doi.org/10.2138/am-2018-6415.
[12] A.C. Deymier, A.K. Nair, B. Depalle, Z. Qin, K. Arcot, C. Drouet, C.H. Yoder, M. J. Buehler, S. Thomopoulos, G.M. Genin, J.D. Pasteris, Protein-free formation of

bone-like apatite: new insights into the key role of carbonation, Biomaterials 127 (2017) 75–88, https://doi.org/10.1016/j.biomaterials.2017.02.029.
[13] M. Okazaki, Y. Moriwaki, T. Aoba, Y. Doi, J. Takahashi, Solubility behavior of CO3 apatites in relation to crystallinity, Caries Res. 15 (1981) 477–483, https://doi.org/10.1159/000260555.
[14] A.A. Baig, J.L. Fox, R.A. Young, Z. Wang, J. Hsu, W.I. Higuchi, A. Chhettry, H. Zhuang, M. Otsuka, Relationships among carbonated apatite solubility, crystallite size, and microstrain parameters, Calcif. Tissue Int. 64 (1999) 437–449, https://doi.org/10.1007/PL00005826.
[15] W.T.R.Z. LeGeros, G. Daculsi, I. Orly, T. Abergas, Solution-mediated transformation of octacalcium phosphate (OCP) to apatite, Scanning Microsc. 3 (1989) 129–138.
[16] S. Ban, M. Matsuura, N. Arimoto, J. Hayashizaki, Y. Itoh, J. Hasegawa, Factors affecting the transformation of octacalcium phosphate to apatite in vitro, Dent. Mater. J. 12 (1993) 106–117271, https://doi.org/10.4012/dmj.12.106.
[17] T. Uchino, C. Ohtsuki, M. Kamitakahara, M. Tanihara, T. Miyazaki, Apatite Formation behavior on tricalcium phosphate (TCP) porous body in a simulated body fluid, Key Eng. Mater. 309–311 (2006) 251–254. https://doi.org/10.4028/www.scientific.net/kem.309-311.251.
[18] R. Rohanizadeh, M. Padrines, J.M. Bouler, D. Couchourel, Y. Fortun, G. Daculsi, Apatite precipitation after incubation of biphasic calcium-phosphate ceramic in various solutions: influence of seed species and proteins, J. Biomed. Mater. Res. 42 (1998) 530–539, https://doi.org/10.1002/(SICI)1097-4636(19981215)42:4<530::AID-JBM8>3.0.CO;2-6.
[19] L.M. Hirakata, M. Kon, K. Asaoka, Evaluation of apatite ceramics containing α-tricalcium phosphate by immersion in simulated body fluid, Bio Med. Mater. Eng. 13 (2003) 247–259.
[20] B. Wingender, M. Azuma, C. Krywka, P. Zaslansky, J. Boyle, A.C. Deymier, Carbonate substitution significantly affects the structure and mechanics of carbonated apatites, Acta Biomater. 122 (2021) 377–386, https://doi.org/10.1016/j.actbio.2021.01.002.
[21] M.M. Moynahan, S.L. Wong, A.C. Deymier, Beyond dissolution: xerostomia rinses affect composition and structure of biomimetic dental mineral in vitro, PLoS One 16 (2021) 5–7, https://doi.org/10.1371/journal.pone.0250822.
[22] M.J. Larsen, A.F. Jensen, D.M. Madsen, E.I.F. Pearce, Individual variations of pH, buffer capacity, and concentrations of calcium and phosphate in unstimulated whole saliva, Arch. Oral Biol. 44 (1999) 111–117, https://doi.org/10.1016/S0003-9969(98)00108-3.
[23] M.J. Larsen, E.I.F. Pearce, Saturation of human saliva with respect to calcium salts, Arch. Oral Biol. 48 (2003) 317–322, https://doi.org/10.1016/S0003-9969(03)00007-4.
[24] E. Lederer, Regulation of serum phosphate, J. Physiol. 592 (2014) 3985–3995, https://doi.org/10.1113/jphysiol.2014.273979.
[25] M.E. Fleet, X. Liu, Location of type B carbonate ion in type A-B carbonate apatite synthesized at high pressure, J. Solid State Chem. 177 (2004) 3174–3182, https://doi.org/10.1016/j.jssc.2004.04.002.
[26] M.E. Fleet, Infrared spectra of carbonate apatites: ν2-Region bands, Biomaterials 30 (2009) 1473–1481, https://doi.org/10.1016/j.biomaterials.2008.12.007.
[27] W.L. Roberts, T.J. Campbell, G.R. Rapp Jr., Encyclopedia of Minerals, second ed., Van Nostrand Reinhold, New York, 1990 https://doi.org/10.1016/0012-8252(75)90109-9.
[28] S. Habelitz, G.W. Marshall, M. Balooch, S.J. Marshall, Nanoindentation and storage of teeth, J. Biomech. 35 (2002) 995–998, https://doi.org/10.1016/S0021-9290(02)00039-8.
[29] A. Secilmis, E. Dilber, N. Ozturk, F.G. Yilmaz, The effect of storage solutions on mineral content of enamel, Mater. Sci. Appl. (2013) 439–445, https://doi.org/10.4236/MSA.2013.47053, 2013.
[30] S. V Dorozhkin, Dissolution mechanism of calcium apatites in acids: a review of literature, World J. Methodol. 2 (2012) 1, https://doi.org/10.5662/wjm.v2.i1.1.
[31] D.A. Bushinsky, Acidosis and bone, in: Nutr. Influ. Bone Heal., 2010, pp. 161–166.
[32] D.A. Bushinsky, Acid-base imbalance and the skeleton, Eur. J. Nutr. 40 (2001) 238–244, https://doi.org/10.1007/s394-001-8351-5.
[33] N. Vandecandelaere, C. Rey, C. Drouet, Biomimetic apatite-based biomaterials: on the critical impact of synthesis and post-synthesis parameters, J. Mater. Sci. Mater. Med. 23 (2012) 2593–2606, https://doi.org/10.1007/s10856-012-4719-y.
[34] C. Rey, C. Combes, C. Drouet, S. Cazalbou, D. Grossin, F. Brouillet, S. Sarda, Surface properties of biomimetic nanocrystalline apatites; Applications in biomaterials, Prog. Cryst. Growth Char. Mater. 60 (2014) 63–73, https://doi.org/10.1016/j.pcrysgrow.2014.09.005.
[35] S. Rowles, in: R. Fearnhead, S. MV (Eds.), Studies on Non-stoichiometric Apatites, John Wright & Sons, Bristol, London, 1964, pp. 56–57, 23–25.
[36] S. Rollin-Martinet, A. Navrotsky, E. Champion, D. Grossin, C. Drouet, Thermodynamic basis for evolution of apatite in calcified tissues, Am. Mineral. 98 (2013) 2037–2045, https://doi.org/10.2138/am.2013.4537.
[37] M. Jarlbring, L. Gunneriusson, W. Forsling, Characterisation of the protolytic properties of synthetic carbonate free fluorapatite, J. Colloid Interface Sci. 285 (2005) 206–211, https://doi.org/10.1016/J.JCIS.2004.11.043.
[38] S. Andrian, S. Stoleriu, Effect of sports and energy drinks on dental hard tissues, in: Sport. Energy Drink., vol. 10, Sci. Beverages, 2019, pp. 339–397, https://doi.org/10.1016/B978-0-12-815851-7.00011-5.
[39] M.J. Larsen, B. Nyvad, Enamel erosion by some soft drinks and orange juices relative to their pH, buffering effect and contents of calcium phosphate, Caries Res. 33 (1999) 81–87, https://doi.org/10.1159/000016499.
[40] R.P. Shellis, M.E. Barbour, A. Jesani, A. Lussi, Effects of buffering properties and undissociated acid concentration on dissolution of dental enamel in relation to ph and acid type, Caries Res. 47 (2013) 601–611, https://doi.org/10.1159/000351641.
[41] C. Combes, S. Cazalbou, C. Rey, Apatite biominerals, Minerals 6 (2016) 34, https://doi.org/10.3390/min6020034.
[42] D.A. Bushinsky, K. Gavrilov, J.M. Chabala, J.D.B. Featherstone, R. Levi-Setti, Effect of metabolic acidosis on the potassium content of bone, J. Bone Miner. Res. 12 (1997) 1664–1671, https://doi.org/10.1359/jbmr.1997.12.10.1664.
[43] C.H. Yoder, M.M. Bollmeyer, K.R. Stepien, R.N. Dudrick, The effect of incorporated carbonate and sodium on the IR spectra of A- and AB-type carbonated apatites, Am. Mineral. 104 (2019) 869–877, https://doi.org/10.2138/am-2019-6800.
[44] D. Laurencin, A. Wong, W. Chrzanowski, J.C. Knowles, D. Qiu, D.M. Pickup, R. J. Newport, Z. Gan, M.J. Duer, M.E. Smith, Probing the calcium and sodium local environment in bones and teeth using multinuclear solid state NMR and X-ray absorption spectroscopy, Phys. Chem. Chem. Phys. 12 (2010) 1081–1091, https://doi.org/10.1039/b915708e.
[45] P. Ptáček, Introduction to apatites, in: Apatites Their Synth. Analog. - Synth. Struct. Prop. Appl., InTech, 2016, https://doi.org/10.5772/62208.
[46] C.H. Yoder, K.R. Stepien, T.M. Edner, A new model for the rationalization of the thermal behavior of carbonated apatites, J. Therm. Anal. Calorim. 140 (2020) 2179–2184, https://doi.org/10.1007/s10973-019-08946-7.
[47] M.E. Fleet, X. Liu, Carbonate in synthetic and biological apatites, in: Ninth Int. Congr. Appl, . Mineral., 2008, pp. 303–311.
[48] S. Peroos, Z. Du, N.H. De Leeuw, A computer modelling study of the uptake, structure and distribution of carbonate defects in hydroxy-apatite, Biomaterials 27 (2006) 2150–2161, https://doi.org/10.1016/j.biomaterials.2005.09.025.
[49] M. Maruta, T. Arahira, K. Tsuru, S. Matsuya, Characterization and thermal decomposition of synthetic carbonate apatite powders prepared using different alkali metal salts, Dent. Mater. J. 38 (2019) 750–755, https://doi.org/10.4012/dmj.2018-213.
[50] C.J.S. Ibsen, H. Leemreize, B.F. Mikladal, J. Skovgaard, M. Bremholm, J. R. Eltzholtz, B.B. Iversen, H. Birkedal, Alkali counterions impact crystallization kinetics of apatite nanocrystals from amorphous calcium phosphate in water at high pH, Cryst. Growth Des. 18 (2018) 6723–6728, https://doi.org/10.1021/acs.cgd.8b01008.